



Salt release from warming sea ice

Karolina Widell,^{1,2} Ilker Fer,¹ and Peter M. Haugan¹

Received 10 March 2006; revised 3 May 2006; accepted 9 May 2006; published 23 June 2006.

[1] In a field study in the Arctic, ejection of dense, saline plumes was observed 1 m below warm land-fast first-year sea ice, under conditions where the heat balance at the ice-ocean interface predicted melting. We describe the observed momentum, heat and salt fluxes in the boundary layer under the ice and the structure of the plume events. Measured downward salt flux was well correlated with upward oceanic heat flux. Our measurements indicate that turbulent heat forcing from below can play an important role for the desalination of warm and saline, hence permeable, sea ice. **Citation:** Widell, K., I. Fer, and P. M. Haugan (2006), Salt release from warming sea ice, *Geophys. Res. Lett.*, 33, L12501, doi:10.1029/2006GL026262.

1. Introduction

[2] The salt content of sea ice highly influences its thermo-dynamical properties, mechanical strength, and electromagnetic properties [Untersteiner, 1986; Carsey, 1992; Leppäranta, 1998]. Despite its importance, the bulk salinity of sea ice is often crudely represented in ice-ocean models [Haarpaintner *et al.*, 2001]. Models providing a high vertical resolution [e.g., Cox and Weeks, 1988] are based on limited laboratory data. Field measurements of sea ice salinity bear large uncertainties due to high spatial variability on small scales [Cottier *et al.*, 1999] and loss of brine during core sampling, especially for ice with high permeability [Notz *et al.*, 2005]. The salt in sea ice is distributed in interstices and channels containing brine surrounded by pure ice. Sea ice is therefore a porous material governed by thermodynamic, chemical and fluid-dynamical processes. In thermal equilibrium, the brine salinity S_{br} is set by the ice temperature T_i via the liquidus (freezing-point) temperature T_f . When the entire pore space is filled with brine and no salt has precipitated as solid crystals, S_{br} is related to the bulk salinity of the ice S_{bu} through $S_{bu} = (1 - \varphi)S_{br}$ where φ is the solid mass fraction.

[3] The conceptual framework provided by the mushy-layer theory has been applied to sea ice [e.g., Wettlaufer *et al.*, 1997]. A mushy layer is a reactive two-phase (porous) medium, where the solid forms a rigid matrix, and the solute-enriched liquid fills, and may flow, within the interconnected interstices [Worster, 1997]. Hence liquid motion is not constrained to the channel systems. A downward motion in the brine channels is compensated by liquid

motion in the other areas of the ice. Horizontal averages of φ , T_i and S_{bu} are continuous functions of the vertical coordinate.

[4] The bulk salinity of multiyear ice is a small fraction of that of seawater, but newly formed ice may have a bulk salinity approaching that of seawater [Notz *et al.*, 2005; Smedsrud and Skogseth, 2006]. Understanding the desalination of young and first year ice is important for both the evolution of its thermal and mechanical properties and for the impact of salt fluxes on ocean stratification, density gradients and circulation. Laboratory experiments suggested that desalination of warming ice is mainly determined from sea-ice state variables [Cox and Weeks, 1975]. In a model study, Vancoppenolle *et al.* [2005] mentioned that brine release reduces the net freshwater flux to the ocean surface layer during melting. Here we present unique observations of brine release from warm first-year land-fast ice subject to forces and conditions similar to those expected for moving sea ice. We discuss the existence and dynamics of such brine release in relation to ocean and sea ice conditions. In addition to the direct relevance for geophysical sea ice properties and under-ice boundary layer turbulence, the observations bear implications for biota in sea ice and biogeochemical fluxes of carbon and other constituents through sea ice.

2. Experiment and Data Processing

2.1. Measurements

[5] Measurements were made of vertical turbulent fluxes of momentum, heat and salt by the eddy-correlation technique using instruments attached to a rigid mast suspended from ~ 1.2 m thick land-fast sea ice in Van Mijenfjorden in Svalbard ($77^\circ 43.00'N$, $15^\circ 10.46'E$). Water depth was 75 m, and the ice was undeformed and of even thickness. Time series of water temperature, T , conductivity, C , and three orthogonal components of velocity were acquired and averaged at 2 Hz by instruments clustered at nominally 1 m and 5 m below the ice. In total, 248 h of data were collected between 11–29 March 2004. In addition to the slow time-response but relatively accurate conductivity units (SBE4C) installed at both levels, a fast-response conductivity sensor (SBE7) mounted at 1 m allows for calculation of the turbulent salinity fluxes. The system is capable of resolving the inertial subrange of turbulence [McPhee, 1992; MCPhee and Stanton, 1996]. Ancillary data obtained next to the under-ice measurement site comprise air temperature at 0.5 m above the ice (12–25 March 2004) and hourly ice temperature (courtesy Knut Høyland) measured by a string of 16 thermistors at 10 cm vertical intervals frozen into the ice on 29 January 2004. The uppermost thermistor was in air, just above the ice surface.

¹Geophysical Institute/Bjerknes Centre for Climate Research, University of Bergen, Bergen, Norway.

²Also at University Centre in Svalbard, Longyearbyen, Norway.

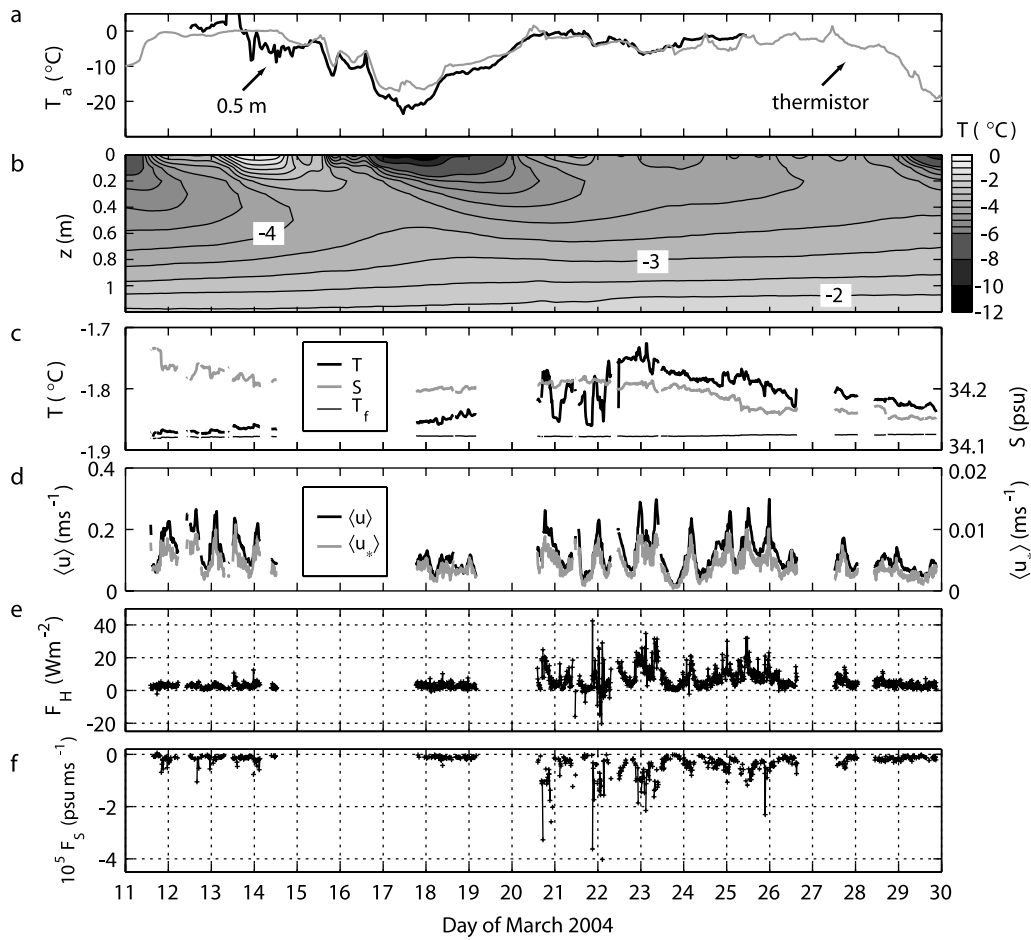


Figure 1. Time series of (a) air temperature, T_a , recorded by the weather station at 0.5 m height (black) and by the uppermost thermistor at the ice surface (gray), (b) isotherms in the ice drawn at 0.5 $^{\circ}\text{C}$ intervals from 0 to -6°C and at 2 $^{\circ}\text{C}$ intervals -6 to -12°C , (c) water temperature at 1 m (black) and freezing point (T_f , thin trace) at local salinity, S (gray) (d) mean longitudinal speed (u , black) and friction speed (u_* , gray), (e) 15-min heat flux, F_H , and (f) salinity flux, F_S .

2.2. Turbulent Fluxes

[6] The calculation of turbulent fluxes follows standard procedures [e.g., *McPhee*, 1992] which involve choosing a suitable averaging period, splitting the measurements into mean and deviatoric (turbulent) quantities and calculating covariances. Synchronized data from the turbulence clusters were segmented at 15-min intervals and the velocity components were aligned such that u , v , and w are the longitudinal, transverse and vertical (positive upward) components and $\langle v \rangle$ and $\langle w \rangle$ vanish. Angle brackets denote averaging. Fluctuating quantities, denoted by prime, are obtained by linearly detrending each segment. Fluxes are obtained by zero-lag covariances invoking Taylor's hypothesis, which states that turbulent features advected past the instruments over a suitable averaging time are representative of the ensemble of instantaneous turbulent fields. Turbulent heat flux is $F_H = \rho C_P \langle w'T' \rangle$, in units of Wm^{-2} , where ρ is the density and C_P is the specific heat of seawater. Reynolds stress per unit mass in complex notation is $\vec{\tau} = \langle u'w' \rangle + i \langle v'w' \rangle$, and local friction speed is $u_* = |\vec{\tau}|^{1/2}$. At 1 m, the instruments are typically in the constant stress

layer and the local u_* is representative of the ice-ocean interface.

2.3. Salinity Calibration

[7] The salinity flux $F_S = \langle w'S' \rangle$, in units of psu m s^{-1} , is sensitive to the absolute salinity and is calculated after careful in situ calibration of the fast response SBE7 against the relatively accurate SBE4C every 15-min: Time series from SBE7 and SBE4C were low-passed at 30-s to account for the slow time response of SBE4C. The records were aligned in time by the lag of maximum correlation (typically 10–30 s, varying at different flow conditions) and averaged at 5 s to reduce noise. By regressing the accurate conductivity record on the SBE7 output signal, new calibration coefficients together with standard error estimates are obtained. Segments for which the lag of maximum correlation is >80 s or for which the calibration coefficient is less than twice the standard error of the estimate are discarded from the analysis. The new calibration coefficients are then applied to the full-scan raw SBE7 output to calculate conductivity. *McPhee and Stanton* [1996] compared values of F_S obtained from SBE4C and SBE7 and reported that the

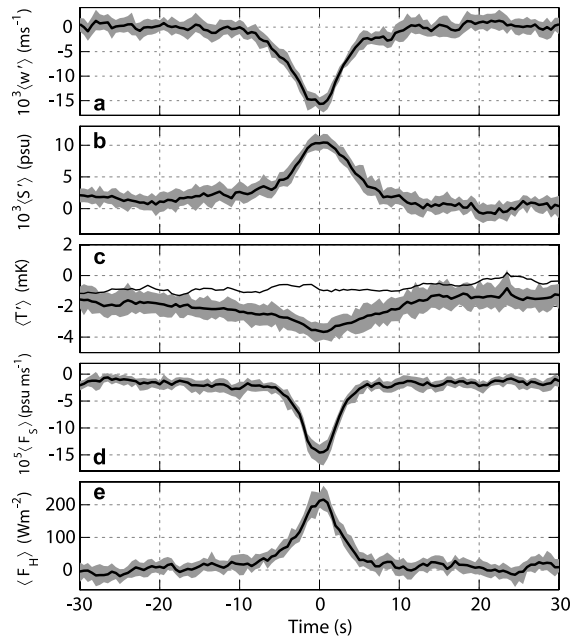


Figure 2. Inferred mean structure of cold, brine plumes over 115 ensembles. Average structures are presented as 1-minute window centered at the time of maximum $|F_S|$. The thick traces are fluctuations of (a) vertical velocity w' , (b) salinity S' , (c) temperature T' and turbulent fluxes of (d) salt $F_S = \langle w'S' \rangle$ and (e) heat, $F_H = \rho C_P \langle w'T' \rangle$, recorded at 1-m below the ice. Gray envelopes are the 95% confidence intervals on the mean. The thin trace in Figure 2c is T' at 5-m below the ice.

standard sensor, which does not adequately resolve the inertial subrange, typically underestimated F_S by 25%. Over 534 calibrated 15-min segments, we find that salt fluxes derived from both sensors are of comparable magnitude and direction and that SBE4C underestimates F_S by 30% on average, lending confidence to our salt flux calculations.

3. Results

[8] During relatively mild atmospheric conditions encountered in Van Mijenfjorden in March 2004 (Figure 1a), the 1.2 m thick ice gradually warmed (Figure 1b). The vertical temperature gradient in the ice implied a positive conductive heat flux of $\sim 6 \text{ W m}^{-2}$ in the bottom 0.2 m of the ice. The water temperature at 1 m (Figure 1c) was close to freezing at the start of the campaign, gradually increased and reached a maximum of $-1.75 \text{ }^\circ\text{C}$, $\sim 0.15^\circ \text{C}$ above T_f , at 23 March. The longitudinal current, $\langle u \rangle$, reached 0.3 m s^{-1} during spring tides and was correlated with u_* throughout the record (Figure 1d) with $\langle u \rangle / u_* = 29 \pm 6$, comparable to other under-ice measurements [McPhee, 2002]. The variability in $\langle u \rangle$ was dominated by tides. Between 20–27 March, F_H at 1 m reached values in excess of 30 W m^{-2} , with an average of 8 W m^{-2} , ~ 3 times that for the remaining portions of the record (Figure 1e). During the same period, negative salt fluxes in excess of $-2 \times 10^{-5} \text{ psu m s}^{-1}$ were measured, with an average of $-5.5 \times 10^{-6} \text{ psu m s}^{-1}$, ~ 1.5 times the survey average. When

derived from hourly ensembles at 5 m below the ice the average temperature was 6 mK warmer, u_* was reduced by 24% and F_H was $\sim 1 \text{ W m}^{-2}$ less than at 1m. Throughout the campaign the positive F_H was correlated with negative F_S (correlation coefficient, $R = -0.7$ using 15-min fluxes), whereas the correlations u_* to F_H and $\langle u \rangle$ to F_H were lower ($R \sim 0.5$).

[9] The mean structure of the strongest brine plumes emanating from the ice can be described by ensemble averaging of large negative salt flux events at 1 m (Figure 2). A brine plume event is detected when $w' < 0$, $S' > 0$ and $|w'S'|$ was greater than five times the rms value over the whole record for at least five consequent scans. This ensures that the detected points are not spikes. Batches of data points of typically 20 scan lengths satisfy these criteria and we delineate an individual event (centre of the brine plume) by choosing the time of maximum $|w'S'|$ within such a segment.

[10] Among a total of 115 identified events, 113 occurred between 20–27 March. Typical duration of a brine plume passage is 20 s, and w' , S' , F_H and F_S show significant peaks at the centre of the plume where downward w' reaches 1.5 cm s^{-1} (Figure 2a and 2b). The positive salinity anomaly is correlated with a negative temperature anomaly at 1 m, which is absent at 5 m (thin trace in Figure 2c), where a clear plume signature was not detected, presumably due to mixing. The cold ($T' < 0$) brine plumes moving downward ($w' < 0$) lead to positive oceanic heat flux signature, reaching on the average $\sim 200 \text{ W m}^{-2}$ with no apparent time lag from the time of maximum negative salt flux (Figure 2d and 2e). This value is a representative instantaneous flux associated with the plume, and does not significantly affect 15-min covariances. The average plume structure is representative of the shape of individual plumes. The time integrated fluxes over the 113 detected plume events account for 4% (11%) of the total F_H (F_S) between 20–27 March.

4. Discussion

[11] Current understanding of salt flux due to heat balance implies that when the oceanic heat flux is higher than the heat conduction, melting will occur at the ice-ocean interface, with subsequent release of meltwater [e.g., *McPhee*, 1992]. However, we observed intensified negative salt flux during such periods, with magnitudes similar to that reported from underneath rapidly freezing leads [*McPhee and Stanton*, 1996]. The correlation between positive oceanic heat flux and negative salt flux indicates a different response to the oceanic turbulent forcing than mere interfacial melting. We suggest that the observed salt flux results from highly permeable, warm sea ice responding to the underlying turbulent flow and in particular to the oceanic heat flux, by release of brine. In contrast to cold sea ice with low volume percentage of highly saline brine, warm sea ice comprises a larger fraction of more diluted liquid. In response to warming, an increasing number of the brine pockets gets interconnected [*Light et al.*, 2003] and permeability increases significantly [*Petrich et al.*, 2006]. Unstable brine density gradients within the interconnected pore space, due to temperature and thereby brine-salinity gradients, will tend to force convective overturning and

release of brine into the ocean [Wettlaufer *et al.*, 2000]. Our observation of persisting correlation between salt and heat fluxes suggests that ocean heat flux controls the permeability and is a controlling parameter for the brine release: As brine drains out of the ice it is replaced by seawater, which, in the absence of a heat supply from below, would lead to internal freeze-up as the lower-salinity seawater encounters temperatures below its liquidus in the ice. This, in turn, would lead to decreased ice permeability and suppress the convection and brine drainage. However, a heat supply from below may prevent this freeze-up and sustain the convection. In Van Mijenfjorden, the necessary heat is supplied by tidal inflows of slightly warmer waters of North Atlantic origin. The cumulative salt release during 21–26 March, the period with largest salt fluxes, is 2.9 kg salt per m². From 1.2 m thick ice, this implies a decrease of around 2.5 psu in mean ice bulk salinity.

[12] Observed salinification of water under drifting Arctic sea ice in conjunction with rafting and ridging of cold ice led Frolov *et al.* [2005] to suggest a mechanism whereby the contact of deeper submerged portions of the ice floes with relatively warmer water results in an increased liquid fraction and brine drainage, consistent with the process reported here.

[13] Feltham *et al.* [2002] suggested a mechanism for mushy layers by which brine flows develop in the ice due to Bernoulli suction by sufficiently rapid oceanic flow. For oceanic shears of 0.2 s⁻¹ at the ice interface, the mechanism is predicted to occur. Average longitudinal current over 15-min segments when 115 identified events occurred is $\langle u \rangle \sim 0.17 \text{ m s}^{-1}$ at 1 m, and assuming zero current at the interface, oceanic shear is comparable to this threshold. Future studies are needed to discern the relative effects of shear, stress, and heat flux to ice desalination.

[14] The integrated positive heat flux caused by the plumes contributes only negligibly to the total heat flux during the periods when the plumes occurred. However a more accurate estimate of the contribution of brine release to the background heat flux requires future experiments. Our contention that the bulk heat flux is determined by background hydrography and mixing, and that the contribution from the plumes is indeed minor is supported by the facts that 15-min mean heat fluxes measured at both levels were comparable in magnitude and could be fairly well reproduced using a bulk formulation [McPhee, 1992]. Crawford *et al.* [1999] observed that advection of horizontal salinity (density) gradients could cause destabilizing buoyancy fluxes near the interface at times when less saline water undercuts more saline water. In our survey, rms salinity differences over 15-min intervals were one order of magnitude less than typical salinity anomaly associated with the plumes. Lack of correlation between the advected horizontal salinity gradient and the measured salt flux indicates that the advective contribution to the measured salt flux is negligible.

5. Concluding Remarks

[15] The development of the sea-ice bulk-salinity profile governs, among other things, the response of sea ice to mechanical deformation and thermal forcing and must be

understood if changes in the Arctic ice cover are to be modeled [Bitz and Lipscomb, 1999]. The measurements reported here show that brine release may occur from first-year fast ice, and probably from first-year moving ice, when relatively warm ice is exposed to an increased oceanic heat flux. This mechanism will affect both the properties of the ice itself and the oceanic mixing in the boundary layer below. The impact on the climatic role of sea ice is unclear. However, from the perspective of a future seasonal Arctic ice cover, the special properties and processes of first-year ice, which may differ substantially from those of the present multiyear Arctic ice sheet, merit further research.

[16] **Acknowledgments.** We thank Dirk Notz, Miles McPhee, Jamie Morison, Frank Nilsen, Povl Abrahamson and Knut Høyland for discussions and contributions to the field campaign. Two anonymous reviewers provided insightful comments. This is publication Nr A 132 of Bjerknes Centre for Climate Research.

References

- Bitz, C. M., and W. H. Lipscomb (1999), An energy-conserving thermodynamic model of sea ice, *J. Geophys. Res.*, *104*, 15,669–15,677.
- Carsey, F. (Ed.) (1992), *Microwave Remote Sensing of Sea Ice*, *Geophys. Monogr. Ser.*, vol. 68, 478 pp., AGU, Washington, D. C.
- Cottier, F., H. Eicken, and P. Wadhams (1999), Linkages between salinity and brine channel distribution in young sea ice, *J. Geophys. Res.*, *104*, 15,859–15,872.
- Cox, G. F. N., and W. F. Weeks (1975), Brine drainage and initial salt entrapment in sodium chloride ice, *Res. Rep. 345*, Cold Reg. Res. and Eng. Lab., Hanover, N. H.
- Cox, G. F. N., and W. F. Weeks (1988), Numerical simulations of the profile properties of undeformed first-year sea ice during the growth season, *J. Geophys. Res.*, *93*, 12,449–12,460.
- Crawford, G., L. Padman, and M. G. McPhee (1999), Turbulent mixing in Barrow Strait, *Cont. Shelf Res.*, *19*, 205–245.
- Feltham, D. L., M. G. Worster, and J. S. Wettlaufer (2002), The influence of ocean flow on newly forming sea ice, *J. Geophys. Res.*, *107*(C2), 3009, doi:10.1029/2000JC000559.
- Frolov, I. E., Z. M. Gudkovich, V. F. Radionov, A. V. Shirochkov, and L. A. Timokhov (2005), *The Arctic Basin: Results from the Russian Drifting Stations*, 272 pp., Springer, New York.
- Haarpaintner, J., J. Gascard, and P. M. Haugan (2001), Ice production and brine formation in Storfjorden, Svalbard, *J. Geophys. Res.*, *106*, 14,001–14,013.
- Leppäranta, M. (Ed.) (1998), *Physics of Ice-Covered Seas*, Helsinki Univ. Press, Helsinki.
- Light, B., G. A. Maykut, and T. C. Grenfell (2003), Effects of temperature on the microstructure of first-year Arctic sea ice, *J. Geophys. Res.*, *108*(C2), 3051, doi:10.1029/2001JC000887.
- McPhee, M. G. (1992), Turbulent heat flux in the upper ocean under sea ice, *J. Geophys. Res.*, *97*, 5365–5379.
- McPhee, M. G. (2002), Turbulent stress at the ice/ocean interface and bottom surface hydraulic roughness during the SHEBA drift, *J. Geophys. Res.*, *107*(C10), 8037, doi:10.1029/2000JC000633.
- McPhee, M. G., and T. P. Stanton (1996), Turbulence in the statically unstable oceanic boundary layer under Arctic leads, *J. Geophys. Res.*, *101*, 6409–6428.
- Notz, D., J. S. Wettlaufer, and M. G. Worster (2005), A non-destructive method for measuring the salinity and solid fraction of growing sea ice in situ, *J. Glaciol.*, *51*, 159–166.
- Petrich, C., P. J. Langhorne, and Z. F. Sun (2006), Modelling the interrelationships between permeability, effective porosity and total porosity in sea ice, *Cold Reg. Sci. Technol.*, *44*, 131–144.
- Smedsrud, L. H., and R. Skogseth (2006), Field measurements of Arctic grease ice properties and processes, *Cold Reg. Sci. Technol.*, *44*, 171–183.
- Untersteiner, N., (Ed.) (1986), *The Geophysics of Sea Ice*, NATO ASI series, Plenum Press, New York.
- Vancoppenolle, M., T. Fichefet, and C. M. Bitz (2005), On the sensitivity of undeformed Arctic sea ice to its vertical salinity profile, *Geophys. Res. Lett.*, *32*, L16502, doi:10.1029/2005GL023427.

Wettlaufer, J. S., M. G. Worster, and H. E. Huppert (1997), Natural convection during solidification of an alloy from above with application to the evolution of sea ice, *J. Fluid Mech.*, *344*, 291–316.

Wettlaufer, J. S., M. G. Worster, and H. E. Huppert (2000), Solidification of leads: Theory, experiment, and field observations, *J. Geophys. Res.*, *105*, 1123–1134.

Worster, M. G. (1997), Convection in mushy layers, *Annu. Rev. Fluid Mech.*, *29*, 91–122.

I. Fer, P. M. Haugan, and K. Widell, Geophysical Institute/Bjerknes Centre for Climate Research, University of Bergen, Allégaten 70, N-5007 Bergen, Norway. (karolina.widell@gf.uib.no)